Measurement of Polydispersity of Ultra-Narrow Polymer Fractions by Thermal Field-Flow Fractionation

MARTIN E. SCHIMPF, MARCUS N. MYERS, and J. CALVIN GIDDINGS, *Department of Chemistry, University of Utah, Salt Lake City, Utah 84112*

Synopsis

In this paper we demonstrate that the polydispersity $\mu = \bar{M}_w/\bar{M}_N$ of narrow polymer fractions can be readily obtained by measuring band broadening and its velocity dependence in a thermal field–flow fractionation (thermal FFF) system. The thermal FFF method is shown to be more accurate than size exclusion chromatography for the determination of polymer polydispersities due to the simpler band dispersion function and the higher selectivity inherent to the technique. The polydispersities of a series of four narrow polystyrene samples prepared by anionic polymerization were consequently determined by thermal FFF and found to be much smaller (1.003–1.006) than the ceiling values (1.06) suggested by the suppliers. As part of this investigation, an experimental study of band dispersion in thermal FFF is used to examine current theory. The data show nonequilibrium to be the dominant factor, whereas relaxation effects are insignificant at lower flow rates and can be subdued at higher flow rates. A high correlation between nonequilibrium theory and experiment allows for the estimation of diffusion coefficients from plate height–velocity data.

INTRODUCTION

In recent years, the field-flow fractionation (FFF) family of techniques has proven applicable to the separation and characterization of a wide range of macromolecular and colloidal materials.[1] Of all the subtechniques of FFF, thermal FFF has been most effectively used for the fractionation of polymers. In thermal FFF, an external "field" in the form of a thermal gradient is applied perpendicular to the flow axis of a narrow ribbon-like channel.[1-3] The velocity profile of fluid moving along the flow axis is near parabolic, with rapid flow in the channel center and reduced flow near the walls. A polymer sample injected into the channel is forced toward the cold wall by thermal diffusion. The resulting buildup of concentration at the cold wall is opposed by ordinary diffusion and a dynamic steady-state condition is reached in which the field-induced motion and back-diffusion are balanced.

In this steady-state condition, the polymer forms a distribution at the cold wall which extends toward the channel center and can be characterized by a mean thickness ℓ, the distance from the cold wall to the center of gravity of the polymer zone. Mean layer thickness ℓ is typically expressed in the dimensionless form $\lambda = \ell/w$, where w is the channel thickness. The ratio ℓ/w or its equivalent λ is called the *retention parameter*, a term of fundamental importance for all FFF techniques.

Parameters ℓ and λ decrease with increasing molecular weight. Because slower flow lines exist toward the channel wall, a compressed high molecular

Journal of Applied Polymer Science, Vol. 33, 117–135 (1987)

CCC 0021-8995/87/010117-19$04.00

weight layer (small λ) will migrate more slowly and be retained longer in the channel than an expanded cloud of low molecular weight polymer molecules. This differential displacement is the basis of fractionation.

The variation of parameter λ among polymers of different molecular weights can be attributed to unequal levels of thermal diffusion and of ordinary diffusion. The relationship of λ to the transport coefficients is given by[4]

$$1/\lambda = w(D_T/D + \gamma)\, dT/dx \tag{1}$$

where D_T and D are the thermal and ordinary diffusion coefficients for the polymer-solvent system, respectively. Parameter γ is the thermal expansion coefficient and dT/dx is the temperature gradient along the axis between channel walls determined by the difference in temperature of the hot and cold walls ΔT.

Parameter λ can also be related, by considering the flow profile existing in the channel, to the retention volume V_r, the volume of carrier liquid required to elute the polymer zone. For parabolic flow[4]

$$R = V^o/V_r = 6\lambda\left[\coth(1/2\lambda) - 2\lambda\right] \tag{2}$$

where R is the retention ratio and V^o is the channel void volume. This equation must be corrected somewhat to account for the departure from parabolic flow induced by the temperature gradient and attendant viscosity changes in the channel.[5]

Thermal FFF has proven to be widely applicable to the characterization of lipophilic polymers. A number of studies have been made on polystyrenes in the molecular weight range from 600 to 20,000,000,[6-9] as well as on polyethylene, polyisoprene, polytetrahydrofuran, and polymethylmethacrylate; this work has been carried out in several different solvents.[4,6,7,10-12] The universal trend is one of increasing retention volume for increased molecular weight. However, the level of retention for each sample varies with the solvent.

Currently, most polymer molecular weight distributions are determined by size exclusion chromatography (SEC). With SEC, one uses molecular weight versus retention volume calibration curves derived from standards whose average molecular weights have been determined by classical methods such as light scattering and osmometry. The elution volume range in SEC is limited to a fraction of the column volume and the applicable molecular weight range for any given column is rigidly fixed. By contrast, with thermal FFF there is no inherent limitation in elution volume range (5–10 channel volumes are often used) and the temperature gradient can be varied widely to provide maximum adaptability to sample type and molecular weight.[13] For high molecular weight polymers, SEC is also hampered by the shear degradation of polymer chains in the high shear flow of the packed bed. The smaller velocity gradient and the absence of extensional shear in the open FFF channel results in greatly reduced shear stress, which is especially advantageous for ultrahigh molecular weight polymers. The absence of packing material also eliminates the need for repeated calibration, required in SEC due to degradation of the packing material.

From the point of view of the present work, the greatest advantage of the uniform open channel used in thermal FFF is the ease of modeling the flow-dependent dispersion processes. The clear distinction between inherent channel dispersion and the dispersion due to sample polydispersity makes it possible to correct for the former and thus to determine accurately the molecular weight distribution, even at low polydispersities. The difficulty in pursuing this goal with SEC lies in the complicated nature of the column dispersion function due to the complex flow pattern inherent in the movement of a fluid through a packed bed. Thus, while thermal FFF yields a simple column dispersion function, that for SEC defies rigorous theoretical formulation.

The dispersion of a solute band in migration through a separation column is characterized by the plate height H, the variance σ_z^2 of the band relative to the distance Z traveled

$$H = \sigma_z^2/Z \tag{2}$$

In the chromatography or FFF of a truly monodisperse sample, the dispersion of the solute during migration is represented by the column or channel contribution H_c. For a polydisperse polymer sample, there is, in addition to column dispersion, a selective dispersion arising from the tendency of the higher molecular weight species to migrate ahead (in the case of SEC) or behind (in the case of thermal FFF) the lower molecular weight species. This polydispersity contribution is represented by H_p. The observed plate height is then the sum of the two terms

$$H = H_p + H_c \tag{4}$$

It is necessary to find a way to decouple the two plate height terms in order to obtain information on polymer polydispersity, available through H_p. Decoupling can be achieved by finding an accurate theoretical value for H_c, or by knowing at least the velocity dependence of H_c, so that H_c can be subtracted from H to yield the desired constant H_p.

The above steps are difficult with SEC because the complexity of flow leads to a complex H_c term. Reasonable theoretical models for the dependence of plate height on mobile phase velocity $\langle v \rangle$ yield expressions that are both complex and inexact. For example, the coupling model of band broadening yields[14]

$$H = H_p + C\langle v \rangle + \Sigma\left[1/(1/A_i + 1/C_i\langle v \rangle)\right] \tag{5}$$

where A_i and C_i are undetermined constants. No practical means exist for isolating small H_p terms from this expression by using $\langle v \rangle$ variations. Polymer standards are not very helpful either because the polydispersities of narrow standards are not known exactly. The substantial uncertainty in H_c is propagated to calculated values of polydispersities. The relative error becomes increasingly large for decreasing polydispersity values, with the literature indicating that μ values below 1.1 are uncertain and those above 1.1 are generally precise to only one place past the decimal.[15-17]

Because of the regular channel geometry of a thermal FFF system, the plate height dependence takes a simple form[18]

$$H = H_p + C\langle v \rangle \tag{6}$$

where C is a constant to be identified later. Isolation of H_p is easily achieved by changing the flow rate of the carrier and extrapolating plate height values to zero velocity. The sensitivity of this method is heightened by the fact that thermal FFF is considerably more selective than SEC[13] and thus yields a relatively larger H_p term. Thus, by using this intercept method, we find that polydispersities can be determined accurately from plate height measurements down to very low values ($\mu < 1.01$).

In this paper, we present the theory and methodology for obtaining polydispersity values of nearly monodisperse polymers using thermal FFF. The general technique was discussed in a previous study on peak broadening in thermal FFF.[19] Although the conditions used in this previous study were less than ideal, results clearly indicated that polydispersity values so obtained are significantly less than the upper limits reported by the manufacturer ($\mu < 1.06$) using SEC. These values are of interest to the polymer theorists concerned with the validity of the Poisson distribution model for living polymerization[20] as well as to experimentalists who rely on narrow polystyrene standards for the calibration of instruments. Our results may also be of interest to those who use narrow polystyrene standards as controls in the development of molecular-weight-sensitive technology. An example is electron-beam microfabrication using positive electron resist polymers where the sensitivity of the resist has been shown to be dependent on molecular weight distribution.[21]

We will extend our study by using the plate height versus velocity data to examine the theoretical model for column dispersion in thermal FFF. We will also determine the feasibility of using the theoretical model to determine polydispersity values from single plate height measurements. Finally, we will compare diffusion coefficients determined experimentally using the plate height theory to those values obtained by other methods.

THEORY

In previous studies we have found that band-broadening processes can be attributed mainly to sample polydispersity represented by H_p, along with nonequilibrium effects and, to a lesser extent, relaxation phenomena,[22,23] the latter two a part of H_c. Plate height contributions from nonequilibrium and relaxation effects have been discussed elsewhere[24] and will be only briefly summarized. A more detailed investigation of the key effect of polydispersity on measured plate height will be presented, however.

Polydispersity

For narrow polymer samples, the polydispersity contribution to peak variance in either SEC or FFF can be represented by

$$\sigma_Z^2 = (dZ/dM)^2 \sigma_M^2 \tag{7}$$

where σ_Z^2 is the longitudinal variance of the solute zone in units of (length)^2, Z is the longitudinal migration distance of a species of molecular weight M, and σ_M^2 is the variance of the molecular weight distribution. Eq. (7) is equivalent to

$$\sigma_Z^2 = Z^2/M^2(d \ln Z/d \ln M)^2\sigma_M^2 \tag{8}$$

Since retention volume V_r is inversely proportional to migration distance Z, Eq. (8) can be rewitten as

$$\sigma_Z^2 = Z^2/M^2(d \ln V_r/d \ln M)^2\sigma_M^2 = Z^2S^2\sigma_M^2/M^2 \tag{9}$$

where $(d \ln V_r/d \ln M)$ is termed the selectivity, S. In thermal FFF, S is approximately constant ($\simeq 0.6$) for a given polymer-solvent system[25] at high retention levels; in SEC, S commonly falls in the range 0.05-0.2.[13]

The term σ_M^2 in Eq. (9) can be expressed as a function of molecular weight averages. The expression will differ for a weight distribution curve, a number distribution curve, etc. The distribution curve should correspond with the property measured by the detector. For the case of a refractometer detector (used in this study and most others), weight is the appropriate distribution to consider. The variance of a weight distribution function $f(M)$ is given by[26]

$$\sigma_M^2 = (\overline{M}_Z/\overline{M}_W - 1)\overline{M}_W^2 \tag{10}$$

where $\overline{M}_Z$ and $\overline{M}_W$ are the z-average and weight-average molecular weights, respectively. By using Eq. (10) in Eq. (9), we obtain

$$\sigma_Z^2 = Z^2S^2(\overline{M}_Z/\overline{M}_W - 1) \tag{11}$$

Using the definition of plate height in Eq. (3) and substituting the channel length L for migration distance Z, we arrive at the following equation

$$H_P = LS^2(\overline{M}_Z/\overline{M}_W - 1) = LS^2(\zeta - 1) \tag{12}$$

Since $\mu = \overline{M}_W/\overline{M}_N$ is more commonly used to express polydispersity than is $\zeta = \overline{M}_Z/\overline{M}_W$, we obtain an expression relating the two and apply it to different distributions. The average molecular weights are defined as[26]

$$\int_0^\infty MN(M)\,dM = \overline{M}_N \tag{13}$$

$$\frac{\int_0^\infty M^2N(M)\,dM}{\int_0^\infty MN(M)\,dM} = \overline{M}_W \tag{14}$$

$$\frac{\int_0^\infty M^3N(M)\,dM}{\int_0^\infty M^2N(M)\,dM} = \overline{M}_Z \tag{15}$$

where $N(M)$ is the normalized number distribution function. From these

expressions the ratio ζ/μ can be written as

$$\frac{\zeta}{\mu} = \frac{\int_0^\infty M^3 N(M) dM \left[\int_0^\infty MN(M)\, dM\right]^3}{\left[\int_0^\infty M^2 N(M)\, dM\right]^3} \tag{16}$$

We will evaluate this ratio for two different polymer distributions.

The polymers used in this study were prepared by anionic techniques. Therefore, the resulting molecular weight distributions are in theory Poisson distributed.[27] We now substitute for $N(M)$ in Eq. (16) the Poisson distribution function

$$N(M) = \frac{e^{-\bar{M}_N} \bar{M}_N^M}{M!} \tag{17}$$

for which the standard deviation is $\sigma_N = \bar{M}_N^{1/2}$. The integrals are evaluated using the expression[26]

$$\sigma_N^2 = (\mu - 1)\bar{M}_N^2 \tag{18}$$

which leads to the following relationship

$$\zeta = \mu\left[\frac{1 + 3(\mu - 1) + 4(\mu - 1)^2}{1 + 3(\mu - 1) + 3(\mu - 1)^2 + (\mu - 1)^3}\right] \tag{19}$$

which, when expanded as a Taylor's series around $\mu = 1$, yields

$$\zeta = 1 + (\mu - 1) + (\mu - 1)^2 + \ldots \tag{20}$$

It is apparent from Eq. (19) that $\zeta > \mu$ when $(\mu - 1) < 1$; since this inequality applies generally to a Poisson distribution, we have in all cases $\zeta > \mu$. Also both ζ/μ and $d\zeta/d\mu$ approach 1 as the distribution approaches monodispersity.

Due to the occurrence of side reactions in the polymerization process, the theoretical Poisson distribution is convoluted with some kinetic dispersion function. Judging from elution peak profiles obtained at low flow rates, where column dispersion is lower than selective dispersion, a Gaussian model is justified. The relation corresponding to Eq. (19) for Gaussian dispersion is found to be

$$\zeta = \mu\frac{1 + 3(\mu - 1)}{1 + 3(\mu - 1) + 3(\mu - 1)^2 + (\mu - 1)^3} \tag{21}$$

which, when expanded around $\mu - 1$ gives

$$\zeta = 1 + (\mu - 1) - 3(\mu - 1)^3 + \cdots \tag{22}$$

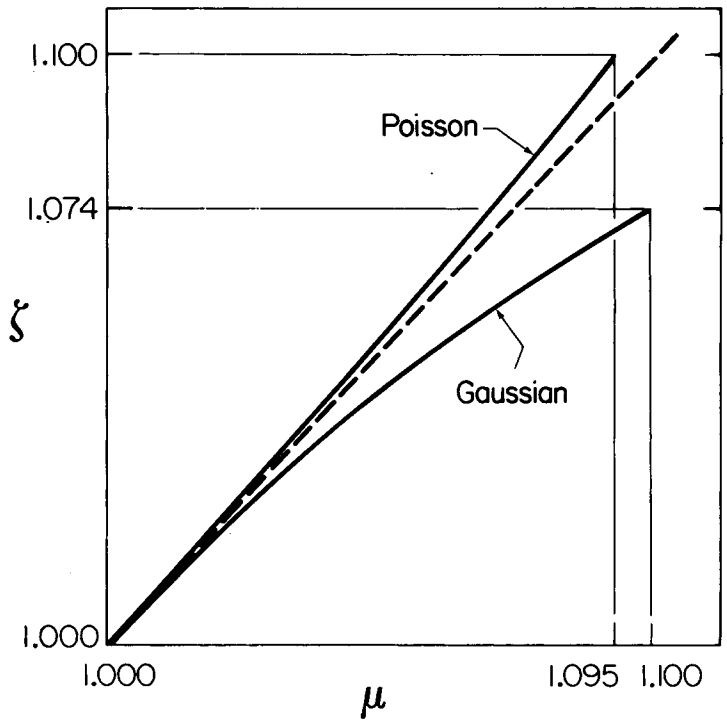

Fig. 1. Plots of $\zeta = \bar{M}_Z/\bar{M}_W$ versus $\mu = \bar{M}_W/\bar{M}_N$ for Poisson and Gaussian number distributions.

Unlike Eq. (19), Eq. (21) yields $\zeta < \mu$ for $(\mu - 1) < 1$. Figure 1 shows plots of μ as a function of ζ for both Eq. (19) and Eq. (21). While these two plots curve away from the $\zeta = \mu$ line in different directions, both approach the $\zeta = \mu$ condition as ζ (and μ) approach unity. As a consequence of this observation, we feel justified in equating ζ and μ for small μ values, say $\mu \leq 1.05$. Thus, under these conditions, the polydispersity contribution to plate height, Eq. (12), can be closely approximated by

$$H_P = LS^2(\mu - 1) \tag{23}$$

Since our derivation has been rather general, this equation should remain applicable to all forms of FFF and to SEC. The various methods differ only in selectivity S.

Column Dispersion

In the absence of axial flow, the thermal gradient-induced drift velocity will be balanced by normal diffusion arising from the concentration gradient established, leading to a steady-state concentration profile at the cold wall. Axial flow upsets the steady state because the nonuniform velocity profile displaces sublayers of the zone unequally. The resulting "nonequilibrium" contribution (H_N) to plate height from this displacement is[28]

$$H_N = \chi w^2 \langle v \rangle / D = C \langle v \rangle \tag{24}$$

where $\langle v \rangle$ is the average mobile phase velocity and χ is a complicated function of the retention parameter λ, approximated by[28]

$$\chi = 24\lambda^3[1 - 8\lambda + 12\lambda^2] \tag{25}$$

When we divide both sides of Eq. (24) by $\langle v \rangle$, we get the C term of Eq. (6). Like Eq. (2), Eq. (25) is based on a parabolic velocity profile across the channel. Perturbation of this profile occurs due to the temperature dependence of the solvent viscosity. The corrected version of Eq. (25) is rather complicated.[5]

While nonequilibrium is the dominant column factor, a second-order "relaxation effect" may also contribute in some circumstances to column dispersion in thermal FFF. During the time required for the polymer zone to "relax" to its steady-state profile at one wall after injection, it is briefly subjected to a greater than normal range of longitudinal flow velocities. The additional plate height from the relaxation effect is approximated by[28]

$$H_r = n(17/140L)\left[w^2\lambda\langle v \rangle/D\right]^2 = E\langle v \rangle^2 \tag{26}$$

where n is the number of relaxation processes occurring in the experiment, presumably one. The relaxation effect gives a slight curvature to the $H - \langle v \rangle$ plots which should be negligible at low longitudinal velocities but significant at higher velocities. In the event that relaxation effects become appreciable, Eq. (6) must be extended due to the addition of Eq. (26) to the following form

$$H = H_P + C\langle v \rangle + E\langle v \rangle^2 \tag{27}$$

However, it is important to note that relaxation effects can be avoided by using a stop-flow procedure in which flow is halted during relaxation.

Finally, the influence of extracolumn volume on plate height can be kept negligible by using the minimum possible lengths of narrow-bore tubing between the sample valve and column head, and between the column outlet and detector cell. Also, the contribution to plate height from longitudinal diffusion is negligible due to the small diffusion coefficients of polymers.

It is apparent from Eqs. (6) and (27) that plots of experimental plate height H as a function of mobile phase velocity $\langle v \rangle$ will yield intercepts equal to the polydispersity contribution to plate height H_P. From known values of the column selectivity and length, the value of the polymer polydispersity can then be determined.

Optimization of Polydispersity Measurement

We can obtain the greatest accuracy in our polydispersity measurement by maximizing the ratio P of the polydispersity plate height contribution to the nonequilibrium contribution. The ratio P is

$$P = \frac{H_P}{C\langle v \rangle} = \frac{LS^2(\mu - 1)}{\chi w^2\langle v \rangle/D} \tag{28}$$

If we approximate[28,4] χ as $24\lambda^3$ and λ by $R/6$, we get

$$P = \frac{9LS^2(\mu - 1)D}{w^2R^3\langle v\rangle} \tag{29}$$

This shows that retention ratio R and channel thickness w are the most effective optimization parameters. Channel thickness should be minimized while the temperature gradient (dT/dx) should be maximized in order to reduce R.

EXPERIMENTAL

The thermal FFF system used in this work consists of two chrome-plated Amzirc bars (a copper-zirconium alloy from Viking Co., Verdi) with highly polished faces clamped together over a 0.003 in (76.2 μm) mylar spacer. The channel dimensions are 2.3 cm in breadth by 34.4 cm in tip-to-tip length (the volume-based length is 31.6 cm). The hot bar was heated by two 1100 W electrical cartridge heaters controlled by computer-activated relay switches. The cold bar has holes drilled through the entire length for cold water flow. Small holes were drilled to within 0.76 mm of the surface of both bars for temperature measurement by an ™Omega (Stamford) thermistor using a copper-constantan thermocouple. Measurements across the length of the channel showed a variation of less than 0.4 K. Variation of hot and cold wall temperatures between experimental runs for any given plate height versus velocity plot was kept at or below 0.2 K.

Two 1-mm holes were drilled in the top copper bar running from the smooth inner face to an outer edge, one at each end, to form the inlet and outlet for the column. The mylar spacer, cut out to form a channel, was positioned so that the two apices formed by the tapered ends aligned with the inlet and outlet holes. The connecting tubing was 0.01 in i.d. stainless steel with a total extra-column volume of approximately 37 μL, or 6% of the void volume. Samples were injected into the flowing solvent at the inlet of the column with a ™Valco (Houston) valve containing a 3 μL cell volume. Polymer concentrations in the sample were typically 2.0 mg/mL.

The samples evaluated are "nearly monodisperse" polystyrenes (specified as $\mu < 1.06$), three of which were obtained from Pressure Chemical Co. (Pittsburgh), the fourth (reported $\bar{M}_W = 179{,}000$) from the National Bureau of Standards. The carrier solvent was ethylbenzene. A gravity pump was used to avoid pulsing. Peak detection was achieved with a Waters Associates (Amherst) R401 Refractive Index Monitor. The retention ratio R was measured by comparing peak elution volumes to that of the void volume obtained from injecting cyclohexane, which is not retained. Two different ΔT values were used to evaluate each polystyrene sample in order to check the consistency of the method. A total of three different ΔT values were used throughout the study. The selectivity S was determined individually for each ΔT by calibration using a series of six narrow polystyrene standards obtained from Pressure Chemical Co. in the molecular weight range from 100,000 to 600,000. At least four measurements were made for each standard for each calibration curve established. Values of λ used for determining the nonequilibrium and relaxa-

tion contributions to plate height were calculated from the measured values of the retention ratio R. For this purpose, we used the expanded form of Eq. (2) which accounts for the influence of the temperature gradient.[5] Values of λ ranged from 0.078 to 0.123 in this study.

Plate heights were calculated using[29]

$$H = \frac{L}{5.54}\left(\frac{t_r}{W_{1/2}}\right)^2 \tag{30}$$

where t_r is the retention time and $W_{1/2}$ is the peak width at half-height measured in the same time units as t_r. Eq. (30) assumes a Gaussian peak profile. A number of experimental peaks were hand digitized and the plate heights calculated using Eq. (3) were compared with those from Eq. (30). The values agreed well in all cases.

Diffusion coefficients (in cm^2/sec) used for the calculation of the nonequilibrium contribution to plate height were approximated by the equation

$$D = (\bar{M}_W)^{-b}\exp(A + C/T) \tag{31}$$

where b, A, and C are 0.552, -3.685, and -1.350, respectively, for polystyrene in ethylbenzene.[30] A comparison of this equation with experimental diffusion coefficients[31-33] shows agreement within 10%.[30]

Finally, a number of stop-flow measurements were made in order to eliminate the plate height contribution $[\langle E\rangle v\rangle^2$ in Eq. (27)] arising from relaxation effects. In these experiments, the flow of carrier was stopped after it had flushed the sample out of the injector and onto the head of the channel. After sufficient time (15–20 sec) was allowed for the transport of the sample to the cold wall under the influence of the thermal gradient, the carrier flow was re-established. This was accomplished with a valve placed in the precolumn tubing just prior to the injection valve.

RESULTS AND DISCUSSION

As previously mentioned, the selectivities S were determined at different ΔT values using a series of six narrow polystyrene standards. The values of ΔT and S are shown in Table I. Here σ represents one standard deviation based on a linear least-squares fit on $\ln V_r$ versus $\ln M$.

Plate height studies were carried out on a series of four narrow polystyrene standards. For each molecular weight, two different ΔT's were used. For each of the eight resulting sets of conditions, a series of plate height measurements

TABLE I
Selectivity S at Different ΔTs

ΔT	$S(\sigma)$
24	0.50 (0.029)
30	0.54 (0.028)
47	0.58 (0.023)

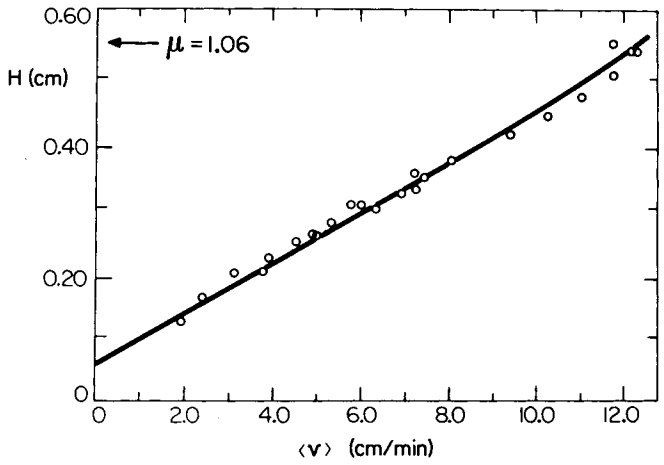

Fig. 2. Plate height vs. carrier velocity. Linear polystyrene $\bar{M}_W$ = 170,000; ΔT = 30 K (T_c = 294 K).

on the elution profiles were made using a range of mobile phase velocities $\langle v \rangle$ from 2 to 12 cm/min. Extreme care was taken to maintain constant ΔT and cold wall temperature T_c.

A typical plate height-velocity plot is shown in Figure 2. An arrow, showing where the intercept would be located for μ = 1.06, demonstrates the extreme departure of these samples from μ = 1.06. The least-squares-acquired parameters for all such samples and plots are summarized in Table II. Here two molecular weight values are given for each polymer. The first value was obtained from λ versus $\bar{M}_W$ calibration curves while the second value in brackets is that reported by the supplier. An examination of polydispersity values evaluated from the intercept term shows that, in three of the four cases, the values obtained using different ΔT's agree quite well. Values obtained for the 200,000 nominal molecular weight polymer are inconsistent, however. This inconsistency will be dealt with later.

The linear C terms show reasonable agreement with those predicted by theory. The experimental values, when not in agreement with theory, are lower. The comparison of theory and experiment is poor for the relaxation term, which fortunately is a second-order term. The theoretical values here were determined assuming the number of relaxations n as one. The n values shown in the table were then obtained by dividing the experimental E values by the theoretical values. Again there are no obvious trends in the comparison except that $n > 1$. This anomalous result may reflect disturbances other than relaxation that have not been accounted for here. The data does confirm that the quadratic term, whatever its origins, is not significant below mobile phase velocities of 6 cm/ min.

Although the second-order effects are minimal in overall plate height calculations, they are detrimental to the acquisition of precise values for the nonequilibrium contribution, which are important for obtaining diffusion coefficients but not for polydispersities. In order to further minimize their influence so that nonequilibrium effects could be studied, two approaches were

TABLE II
Results of Least-Squares Fit of Plate Height Versus Mobile Phase Velocity According to Eq. (27)

$\bar{M}_W$	ΔT (K)	Quadratic Intercept H_p (cm)	Quadratic Intercept $\mu - 1$	Experimental C (min)	Theoretical C (min)	Experimental E (min/cm)	Theoretical E (min/cm)	n
	30	0.0443	0.0048	0.030	0.0358	0.00193	0.00045	4.3
174,000		(0.0031)	(0.0009)	(0.002)		(0.00013)		(0.4)
[179,000]	47	0.0510	0.0048	0.016	0.0163	0.00069	0.00017	4.1
		(0.0044)	(0.0005)	(0.001)		(0.00006)		(0.2)
	30	0.0820	0.0089	0.030	0.0364	0.00064	0.00045	1.4
170,000		(0.0038)	(0.0011)	(0.001)		(0.00005)		(0.1)
[200,000]	47	0.0468	0.0044	0.011	0.0183	0.00057	0.00019	3.0
		(0.0016)	(0.0005)	(0.001)		(0.00002)		(0.1)
	24	0.0680	0.0086	0.032	0.0411	0.00118	0.00071	1.7
295,000		(0.0025)	(0.0013)	(0.001)		(0.00003)		(0.1)
[300,000]	30	0.0680	0.0074	0.019	0.0239	0.00116	0.00037	3.1
		(0.0037)	(0.0008)	(0.001)		(0.000064)		(0.2)
	24	0.0370	0.0047	0.037	0.0392	0.00065	0.00081	1.2
350,000		(0.0077)	(0.0012)	(0.0010)		(0.000024)		(0.1)
[411,000]	30	0.0431	0.0047	0.021	0.0245	0.00097	0.00042	2.3
		(0.0087)	(0.0011)	(0.0012)		(0.00008)		(0.2)

[ ] Supplied by manufacturer.
( ) One standard deviation.

TABLE III
Results of Linear Fit to Plate Height Velocity Data Below Cutoff at $\langle v \rangle \simeq 6$ cm/min

$\overline{M}_W$	ΔT (K)	$\langle v \rangle$ range (cm/min) [no. points]	H_p (cm)	Linear Model $\mu - 1$	Experimental C (min)	Theoretical C (min)
	30	below 5.0	0.0429	0.0047	0.0382	0.0358
174,000		[8]	(0.0060)	(0.0011)	(0.0023)	⟨0.0337⟩
[179,000)	47	below 6.0	0.0537	0.0050	0.0172	0.0163
		[10]	(0.0066)	(0.0006)	(0.0018)	⟨0.0161⟩
	30	below 6.0	0.0649	0.0070	0.0373	0.0364
170,000		[10]	(0.0123)	(0.0022)	(0.0023)	⟨0.0337⟩
[200,000]	47	below 6.0	0.0348	0.0033	0.0178	0.0183
		[6]	(0.0053)	(0.0005)	(0.0013)	⟨0.0177⟩
	24	below 6.0	0.0513	0.0065	0.0412	0.0411
295,000		[5]	(0.0044)	(0.0014)	(0.0014)	⟨0.0398⟩
[300,000]	30	below 5.0	0.0586	0.0064	0.0229	0.0239
		[6]	(0.0039)	(0.0012)	(0.0020)	⟨0.0236⟩
	24	below 6.0	0.0327	0.0041	0.0409	0.0392
350,000		[8]	(0.0049)	(0.0009)	(0.0012)	⟨0.0378⟩
[411,000]	30	below 5.0	0.0282	0.0031	0.0259	0.0245
		[5]	(0.0111)	(0.0015)	(0.0033)	⟨0.0244⟩

( ) One standard deviation.
⟨ ⟩ Isoviscous model.

taken. The first and simplest method was to successfully eliminate the highest velocity data point, fit each new data set to a straight line, and observe the resulting linear term. The upper cutoff velocity where the decrease in the linear term became lost in the random error was between 5 and 6 cm/min for all data sets. Least-squares polydispersity and nonequilibrium C terms resulting from the use of velocities below these cutoff points are displayed in Table III.

The resulting intercept terms are slightly lower than those obtained in the quadratic fit, while the C terms have increased and now show good agreement with theory. An additional set of numbers has been included in brackets in the column of theoretical C values in Table III. These are the theoretical values predicted for a parabolic velocity profile, i.e., those values predicted using Eq. (25) for χ instead of the expanded version given in Ref. 5. These are included to give the reader a feeling for the additional nonequilibrium zone-broadening incurred as a result of the positional dependence of solvent viscosity in the channel.

In a further attempt to eliminate the second-order relaxation effects and thus isolate nonequilibrium zone broadening, three additional data sets were established experimentally. In these cases, the flow of carrier solvent was stopped immediately after sample injection to allow the polymer zone to relax to its steady-state concentration profile at the cold wall and thus eliminate its dispersion due to occupancy of differing flow lines. If relaxation has indeed been made negligible by this stop-flow technique, the plate height-velocity data should lie on a straight line up to the higher velocities used. For each polymer we chose the lower of the two ΔT values used previously because relaxation effects should be greatest for the lower ΔT's. By doing multiple experiments at each velocity, we were able to distinguish random error from systematic error and thus examine the validity of the linear model.

A typical set of stop-flow data is shown in Figure 3 and all results are summarized in Table IV. Correlation coefficients for all plots are high ($r > 0.99$). An F-test confirms the absence of systematic or bias error, thus supporting the validity of the linear model. The polydispersities for 300,000 and 411,000 nominal molecular weight polymers shown in Table IV are in good agreement with those reported in Table III. The polydispersity of the 200,000 nominal molecular weight polymer is significantly lower than that determined by the previous set of experiments at $\Delta T = 30$ K, and is now in much better agreement with the values determined at $\Delta T = 47$ K (Table III). We believe that sample degradation may have been responsible for the high polydispersity value obtained originally on the 200,000 sample at $\Delta T = 30$ K because this particular set of experiments was completed several months after those at $\Delta T = 47$. A fresh solution of the 200,000 sample was therefore prepared for the stop-flow experiments. The lower polydispersity value obtained with the fresh solution supports this hypothesis. The linear C terms in Table IV, like those displayed in Table III, agree well with the values predicted by theory.

The stop-flow results support the validity of the nonequilibrium model, which provide the theoretical C values. Although the C terms determined without stop-flow are consistent with the stop-flow values, the advantage of the latter more tedious method is the better accuracy obtained over a greater range in $\langle v \rangle$, as demonstrated by the lower standard deviations shown in

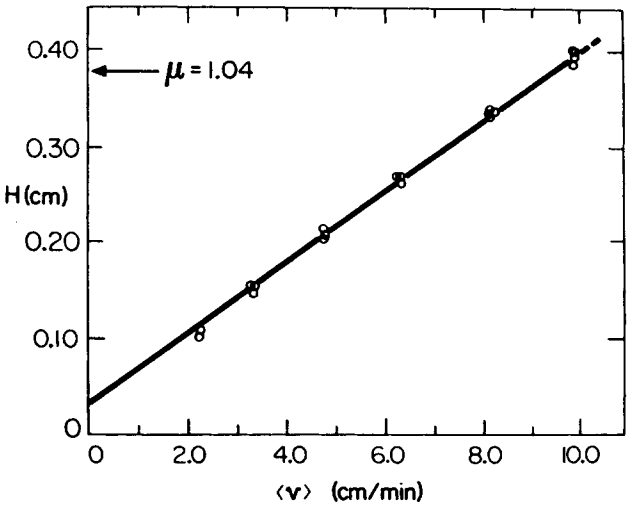

Fig. 3. Plate height vs. carrier solvent velocity with stop-flow. Linear polystyrene $\bar{M}_W$ = 170,000; ΔT = 30 K (T_c = 294 K).

TABLE IV
Results of Linear Fit to Plate Height Velocity Data
Using Stop-Flow Technique

		Stop Flow		Experimental	Theoretical
$\bar{M}_W$	ΔT (K)	H_p (cm)	$\mu - 1$	C (min)	C (min)
170,000	30	0.0311	0.0034	0.0374	0.0364
[200,000]		(0.0077)	(0.0014)	(0.0010)	
295,000	24	0.0433	0.0055	0.0408	0.0411
[300,000]		(0.0093)	(0.0018)	(0.0011)	
350,000	24	0.0468	0.0059	0.0393	0.0392
[411,000]		(0.0087)	(0.0015)	(0.0010)	

( ) One standard deviation.

Table IV. In order to make a direct comparison between this data and that of Table II, we fit the stop-flow data also to a second-order polynomial to examine the quadratic term. The results, displayed in Table V, illustrate the absence of a systematic second-order relaxation effect above the random error of the plate height data.

The nonequilibrium dispersion model provides an independent determination of diffusion coefficients D for dilute polymers. We get D by the rearrangement of Eq. (24).

$$D = \chi w^2 / C \tag{32}$$

Using the experimental C term together with the theoretical χ values, D is immediately calculated. A comparison of D values calculated in this manner with those obtained using Eq. (31) is given in Table VI. Here, the representative temperature is taken as $T(cg)$, the temperature at the center of gravity of

TABLE V
Results of Least-Squares Fit of Plate Height
Versus Mobile Phase Velocity from Stop-Flow Data Using Eq. 927)

$\bar{M}_W$	ΔT (K)	Experimental E (min/cm)	Theoretical E (min/cm)	With stop-flow n	Without stop-flow n
295,000 [300,000]	24	0.000584	0.000713	0.82	1.7
350,000 [411,000]	24	−0.000196	0.000807	−0.24	1.2
170,000 [200,000]	30	−0.000419	0.000446	−0.94	1.4

TABLE VI
Comparison of Diffusion Coefficients Measured from Thermal FFF Data
Using Eq. (32) with Those of Eq. (31)

$\bar{M}_W$	ΔT (K)	$T(cg)$ (K)	D(FFF, Eq. 32) × 10^7 (cm^2/sec)	D(Eq. 31) × 10^7 (cm^2/sec)
174,000	30	298	3.13	3.32
	47	302	3.29	3.58
170,000	30	298	3.18	3.36
	47	302	3.64	3.64
295,000	24	295	2.15	2.34
	30	296	2.46	2.43
350,000	24	294	1.77	2.12
	30	296	2.04	2.21

the solute zone, i.e., at distance ℓ' above the cold wall. The D values determined in this way by thermal FFF are generally within 10% of those values determined independently.

Finally, we would like to examine the feasibility of determining polydispersity values from a single experiment. Plate height intercepts are estimated for each of the eight principal sets of conditions using a single elution profile from each set. For this, we have subtracted out the estimated nonequilibrium contribution using Eq. (31) for D. The resulting H_p values and corresponding polydispersities are shown in Table VII. We have used the experiments run

TABLE VII
Determination of Polydispersity from Single Measurements

$\bar{M}_W$	ΔT (K)	$\langle v \rangle$ (cm/min)	H_p (cm)	$\mu - 1$
174,000	30	2.47	0.0436	0.0056
[179,000]	47	2.39	0.0650	0.0061
170,000	30	2.31	0.0269	0.0035
[200,000]	47	2.45	0.0343	0.0032
295,000	24	2.13	0.0485	0.0061
[300,000]	30	2.45	0.0544	0.0070
350,000	24	2.55	0.0370	0.0047
[411,000]	30	2.45	0.0400	0.0051

nearest to $\langle v \rangle = 2.5$ cm/min for each calculation for the sake of consistency and for the absence of significant relaxation effects. For the three cases where stop-flow experiments were run, we used points from these data sets as opposed to points from the data set without stop-flow. Agreement between data obtained with different ΔT's is good as is agreement between the values in Table VII and those of Tables III and IV. We note that the single experiments used to establish the μ values in Table VII required only 28 to 42 minutes for completion.

CONCLUSIONS

We have found that the polydispersities of narrow polystyrene samples can be consistently obtained in a number of ways from thermal FFF band-broadening data. However, the effect of relaxation and/or some other second-order disturbances on zone broadening is greater than expected and requires careful consideration. The effects are generally negligible and can be avoided in our system at longitudinal velocities below 5 cm/min. Relaxation effects can be eliminated by a stop-flow procedure. When such second-order effects are subdued, nonequilibrium becomes the overwhelming factor in column dispersion. In such cases, the data show high consistency with the model employed here.

Polydispersities obtained by thermal FFF for our limited set of four polymer samples are considerably below the ceiling values ($\mu = 1.06$) reported by the manufacturers. However, they are not as low as theoretically possible for anionic polymerization in the absence of side reactions during polymerization. This limit is given by[34]

$$\mu - 1 = 1/X_N \tag{33}$$

where X_N is the number-average degree of polymerization. Equation (33) would place all μ values well below 1.001. Table VIII summarizes our best estimates for the polydispersities of the polymers used in this study. We believe these values to be accurate to ± 0.002 polydispersity units. However, we cannot presently rule out errors of this magnitude due to dead-volume effects, finite sample size, errors in measuring H, etc.

We note that the difference in precision obtained by using stop-flow methods with a large range of linear velocities as opposed to using a lower range of velocities without stop-flow is not great. This is because the increase in precision from the use of a larger range of $\langle v \rangle$ is offset by a loss of precision due to increased baseline fluctuations typical of the stop-flow experiment. For

TABLE VIII
Summary of Best Estimate of Polydispersities by Thermal FFF

Polymer $\bar{M}_W$		Polydispersity μ	
Supplier	Thermal FFF	Supplier	Thermal FFF
179,000	174,000	< 1.06	1.005
200,000	170,000	< 1.06	1.003
300,000	295,000	< 1.06	1.006
411,000	350,000	< 1.06	1.006

example, if we use a t-table to predict 90% confidence intervals for polydispersities, we find, for the linear extrapolation method without stop-flow, that this interval is ± 0.0016 μ units for the 411,000 nominal molecular weight polymer at a $\Delta T = 24$ K. Using stop-flow for this sample with the same ΔT results in a 90% confidence interval in μ of ± 0.0013. The precision in C, on the other hand, is almost doubled when using the stop-flow method.

For general use, column dispersion in well designed thermal FFF experiments is relatively small at low flow rates, adding 0.01 at most to the uncompensated μ value. Therefore, column contributions can be neglected when measuring μ for relatively polydisperse samples.

In a related study, reasonable values for diffusion coefficients have been determined by thermal FFF from the same experimentally determined values of C used for measuring polydispersity. Although these values have not been extrapolated to infinite dilution, the concentration in the polymer zone is well below the critical concentrations where chain entanglement can occur.[35] In this region, the effect of concentration on diffusion coefficients is not clear. Certain authors have reported an increase in D with concentration[36,37] while others have reported a decrease with concentration.[38] In either case, the reported effect should result in values of D inaccurate by no more than $\pm 10\%$, even if high estimates are used for the zone concentrations. Estimates of D using thermal FFF average 6% below those of Eq. (31).

This material is based upon work supported by grant CHE82-18503 from the National Science Foundation.

References

1. J. C. Giddings, *Sep. Sci. Technol.*, **19**, 831 (1984).
2. J. C. Giddings, M. N. Myers, G. C. Lin, M. Martin, J. Chromatogr. **142**, 23 (1977).
3. S. L. Brimhall, M. N. Myers, K. D. Caldwell, and J. C. Giddings, *Sep. Sci. Technol.*, **16**, 671 (1983).
4. M. N. Myers, K. D. Caldwell, and J. C. Giddings, *Sep. Sci.*, **9**, 47 (1974).
5. J. J. Gunderson, K. D. Caldwell, and J. C. Giddings, *Sep. Sci. Technol.*, **19**, 667 (1984).
6. J. C. Giddings, M. Martin, and M. N. Myers, *J. Chromatogr.*, **158**, 419 (1978).
7. J. C. Giddings, L. K. Smith, and M. N. Myers, *Anal. Chem.*, **48**, 1587 (1976).
8. J. C. Giddings, L. K. Smith, and M. N. Myers, *Anal. Chem.*, **47**, 2389 (1975).
9. Y. S. Gao, K. D. Caldwell, M. N. Myers, and J. C. Giddings, *Macromolecules*, **18**, 1272 (1985).
10. G. H. Thompson, M. N. Myers, and J. C. Giddings, *Anal. Chem.*, **41**, 1219 (1969).
11. J. C. Giddings, M. N. Myers, and J. Janca, *J. Chromatogr.*, **186**, 261 (1969).
12. M. Martin and R. Reynauld, *Anal. Chem.*, **52**, 2293 (1980).
13. J. C. Giddings, Y. H. Yoon, and M. N. Myers, *Anal. Chem.*, **47**, 126 (1975).
14. J. C. Giddings, *Dynamics of Chromatography*, Marcel Dekker, New York, 1965.
15. F. L. McCrackin, *J. Appl. Polym. Sci.*, **21**, 191 (1977).
16. M. Hess and R. F. Kratz, *J. Polym. Sci.*, **A-2,4**, 731 (1966).
17. A. R. Cooper, J. F. Johnson, and A. R. Bruzzone, *Eur. Polym. J.*, **9**, 1393 (1973).
18. J. C. Giddings, *Sep. Sci.*, **8**, 567 (1973).
19. M. Martin, M. N. Myers, and J. C. Giddings, *J. Liq. Chromatogr.*, **2**, 147 (1979).
20. P. Flory, *J. Am. Chem. Soc.*, **62**, 1561 (1940).
21. J. H. Lai and L. Shepherd, *J. Appl. Polym. Sci.*, **20**, 2367 (1976).
22. L. K. Smith, M. N. Myers, and J. C. Giddings, *Anal. Chem.*, **49**, 1750 (1977).
23. M. E. Hovingh, G. H. Thompson, and J. C. Giddings, *Anal. Chem.*, **42**, 195 (1970).

24. L. K. Smith, M. N. Myers, and J. C. Giddings, *Anal. Chem.*, **49**, 1750 (1977).
25. J. C. Giddings, M. N. Myers, and J. Janca, *J. Chromatogr.*, **186**, 37 (1979).
26. L. H. Tung, in *Polymer Fractionation*, M. J. R. Cantow, ed., Academic Press, New York, 1967, p. 379.
27. P. J. Flory, *Principles of Polymer Chemistry*, Cornell University Press, Ithaca, N. Y., 1953, p. 266.
28. J. C. Giddings, Y. H. Yoon, K. D. Caldwell, M. N. Myers, and M. E. Hovingh, *Sep. Sci.*, **10**, 447 (1975).
29. L. R. Snyder and J. J. Kirkland, *Introduction to Modern Liquid Chromatography*, 2nd ed., John Wiley, New York, 1979, p. 222.
30. J. C. Giddings, K. D. Caldwell, and M. N. Myers, *Macromolecules*, **9**, 106 (1976).
31. F. Meyerhoff and K. Nachtigall, *J. Polym. Sci.*, **57**, 227 (1962).
32. V. Bugdahl, *Kautsch. Gumme, Kunstst.*, **22**, 486 (1969).
33. D. L. Taylor, *J. Polym. Sci., Part*, **A-2**, 611 (1964).
34. M. Ezrin, *Polymer Molecular Weight Methods*, Advances in Chemistry Series 125, American Chemical Society, Washington, D. C., 1973.
35. S. Brimhall, Y. S. Gao, K. D. Caldwell, and J. C. Giddings, in preparation.
36. H. Matsuda, H. Aonuma, and S. Kuroiwa, *J. Appl. Polym. Sci.*, **14**, 335 (1970).
37. C. Beckman and J. C. Rosenberg, *Ann. NY Acad. Sci.*, **46**, 329 (1945).
38. M. J. Schick, doctoral thesis, Polytechnical Institute, 1949.

Received March 18, 1986
Accepted May 14, 1986